Journal of
Synchrotron
Radiation

ISSN 0909-0495

Received 4 April 2007
Accepted 13 September 2007

X-ray diffractometry and topography of lattice plane curvature in thermally deformed Si wafer

J. M. Yi,[a]‡ Y. S. Chu,[b] T. S. Argunova,[a,c] J. Z. Domagala[d] and J. H. Je[a]*

[a]X-ray Imaging Center, POSTECH, Pohang 790-784, Korea, [b]Advanced Photon Source, Argonne National Laboratory, Argonne, IL 60439, USA, [c]Ioffe Physico-Technical Institute, RAS, St Petersburg, Russia, and [d]Institute of Physics, Polish Academy of Sciences, Al. Lotnikow 32/46, 02-668 Warszawa, Poland. E-mail: jhje@postech.ac.kr

The correlation between the microscopic lattice plane curvature and the dislocation structure in thermal warpage of 200 mm-diameter Czochralski Si (001) wafers has been investigated using high-resolution X-ray diffractometry and topography. It is found that the (004) lattice plane curvature is locally confined between two neighboring slip bands, with the rotation axis parallel to the slip bands. High-resolution topography reveals that the curvature resulted from a fragmented dislocation structure. The local confinement is attributed to the multiplication of the dislocations that are generated between the two slip bands.

Keywords: imaging; diffraction.

1. Introduction

Wafer warpage owing to thermal stress in a very large scale integrated-circuit fabrication is a rediscovered issue of concern at each step of Si wafer enlargement (Hu, 1973; Leroy & Plougonven, 1980; Widmer & Rehwald, 1986; Sueoka *et al.*, 1997; Fischer *et al.*, 2000). Extensive efforts have been devoted to elucidate the onset mechanism of wafer warpage with an emphasis on the distribution of thermal stress within a wafer (Hu *et al.*, 1976; Bentini *et al.*, 1984) and/or on the effect of oxygen precipitates that are incorporated by the precipitation treatments (Leroy & Plougonven, 1980; Fukuda & Moizuka, 1992; Chiou *et al.*, 1994). The experimental and theoretical results have shown that the macroscopic shape, saddle or cup-type in thermally warped Si wafers depends on the tensile or compressive stress during thermal treatments. Such macroscopic wafer warpage is often related to the multiplication of dislocations that are generated from the oxygen precipitates or the punched-out dislocations (Sueoka *et al.*, 1997) around them. However, the detailed mechanism by which the dislocations induce the microscopic lattice plane curvature in the warpage is not fully understood.

In this article we investigate the correlation between the lattice plane curvature and the dislocation structure in thermally deformed saddle-shaped Si (001) wafers using high-resolution X-ray diffractometry and topography. We find that the (004) lattice plane curvature is locally confined between two neighboring slip bands that are facing each other. The local confinement is discussed with the formation of a fragmented dislocation structure that is developed between the two slip bands.

‡ Present address: Advanced Photon Source, Argonne National Laboratory, Argonne, IL 60439, USA.

2. Experimental

Thermal tests of 200 mm-diameter single-side-polished dislocation-free Czochralski Si (001) wafers [p-type (0.015 Ω cm), 750 μm thick] were performed at 1423 K for 10 min, which is equivalent to the thermal conditions of Si epitaxy in LSI processing. Saddle-type warpage, which was observed by a standard flatness tester, was generated owing to the radial stress induced by the thermal gradient. Line patterns (surface features of slip bands) appeared at the wafer edges of the $\pi/8$ and $\langle 110 \rangle$ zones with 45° periodicity (Hu *et al.*, 1976), extending into the center along the $\langle 110 \rangle$ direction with length 25–30 mm. The slip bands were observed as a pair with a separation distance of about 1 mm, as confirmed by optical microscope (inset of Fig. 1*a*), and with a density of the pairs of 1/30°. A 40 mm × 40 mm sample was prepared from one of the concave regions with a reference of the polished side of the wafer by carefully cutting the wafer along the orthogonal $\langle 110 \rangle$ directions.

To investigate the spatial distribution of lattice plane curvature around the slip bands, high-resolution diffractometry experiments were performed using the conventional X-ray source of Cu $K\alpha_1$. A triple-axis configuration (Bowen & Tanner, 1998) with an asymmetric four-bounce Ge (220) monochromator and a Ge (220) channel-cut analyzer was applied to obtain high angular resolution. In particular, for high spatial resolution, the X-ray beam size was controlled to 10 μm horizontally by 100 μm vertically using a beam aper-

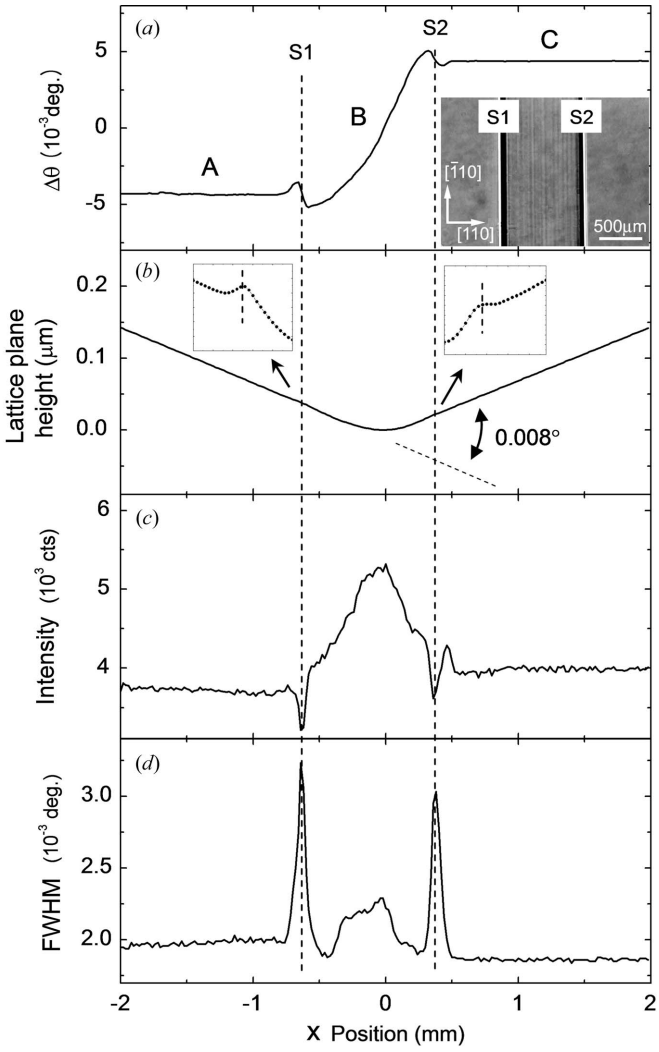

Figure 1
The profiles of (*a*) Si (004) lattice misorientation, (*c*) peak intensity and (*d*) FWHM of the Si 004 θ rocking series, as a function of the [110] position across the two slip bands (S1 and S2) shown in the optical micrograph [the inset to (*a*)]. (*b*) Profile of 'lattice plane height' variation, calculated from (*a*), showing the cross-sectional view of the Si (004) lattice plane profile in real space. The insets to (*b*) show enlarged views around the slip bands.

ture. The symmetric Si 004 reflection was used for the diffraction measurements. The slip bands of the sample were set perpendicular to the horizontal direction of the beam. A series of θ rocking measurements for the 004 reflection were conducted while translating the sample horizontally in a position step of 20 μm across the two neighboring slip bands.

High-resolution topography experiments (Authier, 2001) using synchrotron X-rays were also performed at the XOR 2-BM beamline of the Advanced Photon Source, USA. A monochromatic beam was provided by a Si (111) double-bounce monochromator at 15 keV. The sample was set to a symmetric Si 004 reflection ($\theta = 17.7^\circ$) in the Bragg geometry. An optically coupled high-resolution CCD camera system (Koch *et al.*, 1998) was used for imaging the diffracted beam intensity. The CCD system was set up normally to the diffracted beam and positioned 5 mm away from the sample. Synchrotron white-beam topography experiments using the Laue geometry were additionally carried out at the 7B2 beamline of the Pohang Light Source, Korea (Yi *et al.*, 2005).

3. Results and discussions

From longitudinal scan measurement of the Si 004 reflection by X-ray diffractometry, we observed no existence of the (004) lattice variation, indicating that the strain associated with the thermal process was fully relaxed by plastic deformation. Fig. 1(*a*) shows the profile of the Si (004) lattice misorientation, which was obtained at the wafer edge by the X-ray diffractometry measurements, as a function of the position along the [110] direction perpendicular to the slip bands. Here the '$\Delta\theta$–x' curve implies the spatial distribution of the Si (004) lattice orientation across the two slip bands. The lattice orientation distribution exhibits three particular patterns: dipole-shaped (around S1 and S2), flat (regions A and C) and parabolic (region B). The lateral distance between the positions of the two dipole-shaped patterns is about 1 mm, identical to the separation of the two slip bands observed in the optical micrograph, indicating that the two dipole-shaped patterns are due to the two slip bands.

To express the configuration of the Si (004) lattice plane curvature in real space, we calculated the lattice plane profile using a simple relation. The lattice misorientation, $\Delta\theta(x)$, is associated with the 'lattice plane height' function, $z(x)$, by the equation $z(x+1) - z(x) = \tan[\Delta\theta(x)]\Delta x$, where x is the lateral coordinate. From the '$\Delta\theta$–x' profile of Fig. 1(*a*), we obtained the 'lattice plane height' *versus* position, as shown in Fig. 1(*b*), with the reference of the center position between the two slip bands. The figure in fact shows the cross-sectional view of the Si (004) lattice plane profile. From the concave regions of the sample, we find that the curvature is locally confined within the region between the two slip bands, with the $[\bar{1}10]$ rotation axis parallel to the slip bands. As shown in Figs. 1(*a*) and 1(*b*), the two regions (A and C) outside the two slip bands show flat lattice plane profiles, indicating no lattice plane curvature. The concave curvature exists only in the region (B) between the two slip bands. From the misorientation angle of 0.008° between the two flat regions, the calculated radius of the local curvature is as small as $\sim$7 m, indicating that the curvature was formed with significant strain localization between the two slip bands.

The profiles of the peak intensity (Fig. 1*c*) and the full width at half-maxima (FWHM) (Fig. 1*d*) of the series of the θ rocking measurements also demonstrate the local confinement of the lattice plane curvature. The FWHMs in the regions A and C are as extremely low as $\sim$0.002°, which corresponds to that of a perfect Si single crystal, and the peak intensities are almost constant and low, indicating no plastic deformation in the two regions. Meanwhile, the region B exhibits enhanced peak intensities and high FWHMs. Such simultaneous increase of the intensity and the FWHM in the region B is consistent with the existence of the concave lattice plane curvature. On the other hand, the two slip bands S1 and S2 show the opposite

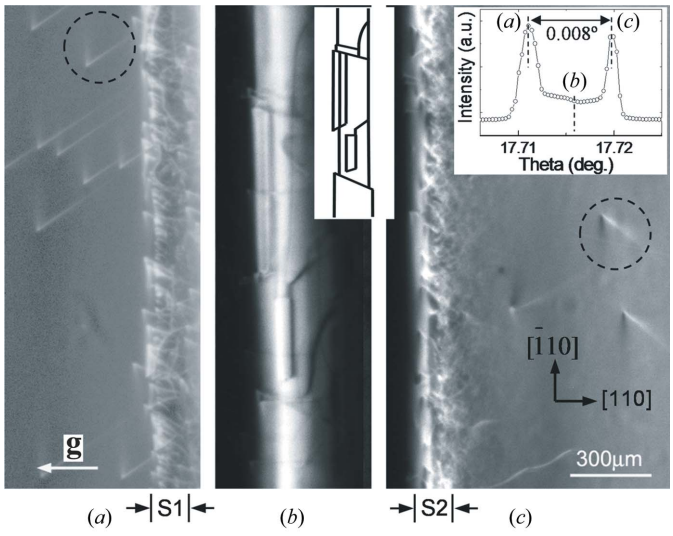

Figure 2
Three X-ray topographs (g = 004) obtained by rocking-curve imaging, representing three local regions of the Si sample. The corresponding θ angles are indicated on the rocking curve [the inset to (c)]. Note the fragmented dislocation structure in (b), as schematically shown in the inset.

trend between the FWHM and the peak intensity, possibly indicating the presence of dislocations.

To reveal the dislocation structure associated with the slip bands and the curvature formation, high-resolution synchrotron X-ray topography was performed for the same sample region of Fig. 1. The rocking-curve imaging method (Lübbert *et al.*, 2000) was applied to meet the Si (004) lattice misorientation. Figs. 2(a)–2(c) show three different topographic images, representing three different local regions of the sample, where the corresponding θ angles are marked on the rocking curve (the inset to Fig. 2c). In the figures the inclined lines of the hook-shape features (dotted circles) indicate dislocations, while the vertical lines are due to diffraction contrast at the surface exits of the dislocations. Slip bands are clearly seen with high density of dislocations with arrays at S1 and S2. Note that the two regions outside the slip bands, in Figs. 2(a) and 2(c), show few defects and homogeneous intensity, indicating no plastic deformation, consistent with the result of X-ray diffractometry in Fig. 1. Interestingly, Fig. 2(b) shows a network of lines, as schematically illustrated in the inset. This indicates the formation of a fragmented dislocation structure (Hughes, 1993) in the region. From the correlation between the lattice plane profile (Fig. 1) and the dislocation structure (Fig. 2), we conclude that the formation of the lattice plane curvature resulted from the fragmented dislocation structure within the region between the two slip bands. The low density of the fragmented dislocation boundaries of $\sim$0.01 μm^{-1}, compared with the large misorientation angle of 0.008°, indicates that the boundaries are composed of multiple dislocations piled up along the thickness direction (density $\sim$0.1 μm^{-1}).

To elucidate the dislocation mechanism of the slip bands, we investigated the leading dislocations. Fig. 3(a) shows an X-ray

Table 1
Summary of the dislocation line directions **l**, and the Burgers vectors **b**, of the studied dislocations.

Mark	**l**	Reflections **g** invisible	**b**	Slip plane
A	[1̄01]	511; 5̄11	±[01̄1]	(111)
B	[011]	1̄51; 5̄11	±[101]	(1̄1̄1)
C	Curved	151; 1̄51	±[1̄01]	(111)

topograph obtained in the region 30 mm from the wafer edge. Two leading dislocations (black lines), labeled A and B, are characterized as parallel arrays and thickness-wise propagation, clearly showing the features of the slip bands. The dislocations were characterized by the rotation method (Yi *et al.*, 2006) and white-beam topography, as summarized in Table 1. The slip planes were identified as (111) and (1̄1̄1), which are facing each other, forming a pyramidal section of the wafer, as schematically shown in Fig. 3(b). The Burgers vectors were identified as ⟨01̄1⟩ and ⟨1̄01⟩ types. The inclination of the two Burgers vectors to the surface implies that the

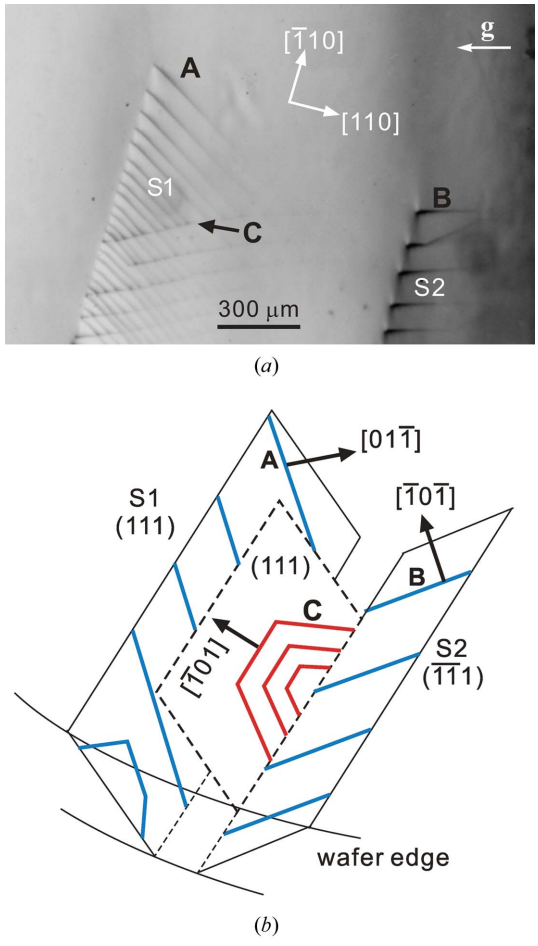

Figure 3
(a) X-ray topograph (g = 004) showing the dislocation structure of the leading head of the two slip bands S1 and S2. (b) Schematic representation of multiplication of the dislocations necessary for the fragmented dislocation structure.

pyramidal section moved vertically forming the surface steps, as confirmed by the lattice plane profile in the inset to Fig. 1(*b*).

We now discuss the formation mechanism of the fragmented dislocation structure. It is reasonable that the vertical movement of the pyramidal section results in elastic bowing of the wafer, inducing strain localization on it. Together with the long-range strain fields of the slip bands (Hull, 1975), the strain localization can activate dislocation sources within the slip bands, such as oxygen precipitates, and/or primary slip dislocations. Then dislocation loops produced by the sources may expand and multiply in crossed slip planes (Hirth & Lothe, 1982), such as the dotted square (111) plane in Fig. 3(*b*), forming the arrays of the dislocations of the same sign, and as a result the fragmented dislocation structure.

4. Conclusion

We have investigated the correlation between the lattice plane curvature and the dislocation structure in the thermally deformed saddle-shaped Si wafer using high-resolution X-ray diffractometry and topography. It was found that the lattice plane curvature was locally confined between two slip bands that form the pyramidal section in the wafer. The curvature formation resulted from the fragmented dislocation structure. The local confinement is attributed to the multiplication of the dislocations that are generated between the two slip bands.

This research was supported by the Creative Research Initiatives (Functional X-ray Imaging) of MOST/KOSEF. Use of the Advanced Photon Source was supported by the US Department of Energy, Office of Science, Office of Basic Energy Sciences, under Contract No. DE-AC02-06CH11357.

References

Authier, A. (2001). *Dynamical Theory of X-ray Diffraction.* Oxford University Press.
Bentini, G., Correra, L. & Donolato, C. (1984). *J. Appl. Phys.* **56**, 2922–2929.
Bowen, D. K. & Tanner, B. K. (1998). *High-Resolution X-ray Diffractometry and Topography.* London: Taylor & Francis.
Chiou, H.-D., Chen, Y., Carpenter, R. W. & Jeong, J. (1994). *J. Electrochem. Soc.* **141**, 1856–1862.
Fischer, A., Richter, H., Kurner, W. & Kucher, P. (2000). *J. Appl. Phys.* **87**, 1543–1549.
Fukuda, T. & Moizuka, M. (1992). *Appl. Phys. Lett.* **60**, 1184–1186.
Hirth, J. P. & Lothe, J. (1982). *Theory of Dislocations.* New York: John Wiley and Sons.
Hughes, D. A. (1993). *Acta Metall. Mater.* **41**, 1421–1430.
Hull, D. (1975). *Introduction to Dislocations.* Oxford: Pergamon Press.
Hu, S. M. (1973). *Appl. Phys. Lett.* **22**, 261–264.
Hu, S. M., Klepner, S. P., Schwenker, R. O. & Seto, D. K. (1976). *J. Appl. Phys.* **47**, 4098–4106.
Koch, A., Raven, C., Spanne, P. & Snigirev, A. (1998). *J. Opt. Soc. Am. A*, **15**, 1940–1951.
Leroy, B. & Plougonven, C. (1980). *J. Electrochem. Soc.* **127**, 961–970.
Lübbert, D., Baumbach, T., Härtwig, J., Boller, E. & Pernot, E. (2000). *Nucl. Instrum. Methods*, B**160**, 521–527.
Sueoka, K., Akatsuka, M., Katahama, H. & Adachi, N. (1997). *J. Electrochem. Soc.* **144**, 1111–1120.
Widmer, A. E. & Rehwald, W. (1986). *J. Electrochem. Soc.* **133**, 2403–2409.
Yi, J. M., Chu, Y. S., Argunova, T. S. & Je, J. H. (2006). *J. Appl. Cryst.* **39**, 106–108.
Yi, J. M., Seol, S. K., Je, J. H., Argunova, T. S., Hwu, Y. & Tsai, W.-L. (2005). *Nucl. Instrum. Methods*, A**551**, 152–156.